Continental Shelf Research 29 (2009) 1251–1263

Contents lists available at ScienceDirect

Continental Shelf Research

journal homepage: www.elsevier.com/locate/csr

High-frequency vertical current observations in stratified seas

Hans van Haren

Royal Netherlands Institute for Sea Research (NIOZ), P.O. Box 59, 1790 AB Den Burg, the Netherlands

ARTICLE INFO

Article history:
Received 15 August 2008
Received in revised form
26 January 2009
Accepted 9 February 2009
Available online 20 February 2009

Keywords:
Vertical motions
High-frequency waves
Low-modes
ADCP-observations

ABSTRACT

Although large-scale tidal and inertial motions dominate the kinetic energy and vertical current shear in shelf seas and ocean, short-scale internal waves at higher frequencies close to the local buoyancy frequency are of some interest for studying internal wave breaking and associated diapycnal mixing. Such waves near the upper limit of the inertio-gravity wave band are thought to have relatively short O (10^2–10^3 m) horizontal scales and to show mainly up- and downward motions, which contrasts with generally low aspect ratio large-scale ocean currents. Here, short-term vertical current (w) observations using moored acoustic Doppler current profiler (ADCP) are presented from a shelf sea, above a continental slope and from the open ocean. The observed w, with amplitudes between 0.015 and 0.05 m s^{-1}, all span a considerable part of the water column, which is not a small vertical scale O(water depth) or O (100–500 m, the maximum range of observations), with either 0 or π phase change. This implies that they actually represent internal waves of low vertical modes 1 or 2. Maximum amplitudes are found in layers of largest stratification, some in the main pycnocline bordering the frictional bottom boundary layer, suggesting a tidal source. These 'pycnocline-w' compose a regular train of (solitary) internal waves and linearly decrease to small values near surface and bottom.

1. Introduction

Vertical currents (w) have not been frequently measured in the ocean or shelf seas, because their amplitude is generally small compared to that of horizontal current components (u, v) as a result of the O (10^{-3}) aspect ratio $|w|/|u, v|$ on relatively large basin-wide scales. However, the aspect ratio can become $O(1)$ and w-amplitudes $O(10^{-2}$–$10^{-1})$ m s^{-1} on small internal wave and large, not dissipation, near-turbulence scales. However, at these scales w is also somewhat difficult to measure with standard ocean current observing equipment that does not resolve the adequate time O (1–100 s) and space O (1–100 m) scales of motions that can be modulated at tidal or longer time scales. Although variations at such small scales have been observed using high-resolution temperature sensors (e.g., Halpern, 1971; Thorpe, 1987; Marmorino et al., 1987), the lack of w-measurements hampers studies on diapycnal turbulent mixing. This importance of w-measurements for vertical mixing has been demonstrated using, rare, ship borne acoustic observations that did resolve the above scales (e.g., Gargett and Moum, 1995; Klymak and Moum, 2003) and using moored instrumentation in areas of dense deep-water formation or convective mixing (e.g., Schott and Leaman, 1991).

Of particular interest in studying diapycnal mixing is the relation between, the breaking of, short-scale internal waves, which are characterized by relatively large w, and large-scale convection, or, vertical variation of large-scale horizontal current. The latter is characterized by shear $\mathbf{S} = (\partial u/\partial z, \partial v/\partial z)$. The problem of such a study is that internal wave breaking occurs infrequently, so that high-resolution sampling is needed over a prolonged period of time O(weeks–months).

With the advent of ever-increasing internal data storage capacities it is now becoming possible to study w at sufficient resolution over a prolonged period of time in a mooring array, e.g. demonstrating the importance of highly non-linear 'solitary' bore-like waves very near the buoyancy frequency N that dominate sediment transport up sloping bottoms (Hosegood et al., 2004). Debate is ongoing how these waves and their large w, indeed having $O(0.1$ m s$^{-1})$ amplitudes extending over O(10–100 m) vertically, affect the average vertical exchange and associated dissipation of large-scale [tidal] energy. Short-term large w is observed sweeping up resuspended material 10's of meters away from the sea floor.

In the present paper, examples of securely moored four-beam acoustic Doppler current profiler (ADCP)-observations are presented to learn more about details of [beam-averaged] w associated with high-frequency internal waves in a shelf sea, above a continental slope and in the deep ocean. The ADCP's are either fixed to the bottom, in the stratified shelf sea during calm summer period, or mounted in a heavy top-buoy far below the influence of surface waves. In these set-ups, the instruments cannot alias surface wave action to a significant extent.

E-mail address: hansvh@nioz.nl

0278-4343/$ - see front matter © 2009 Elsevier Ltd. All rights reserved.
doi:10.1016/j.csr.2009.02.002

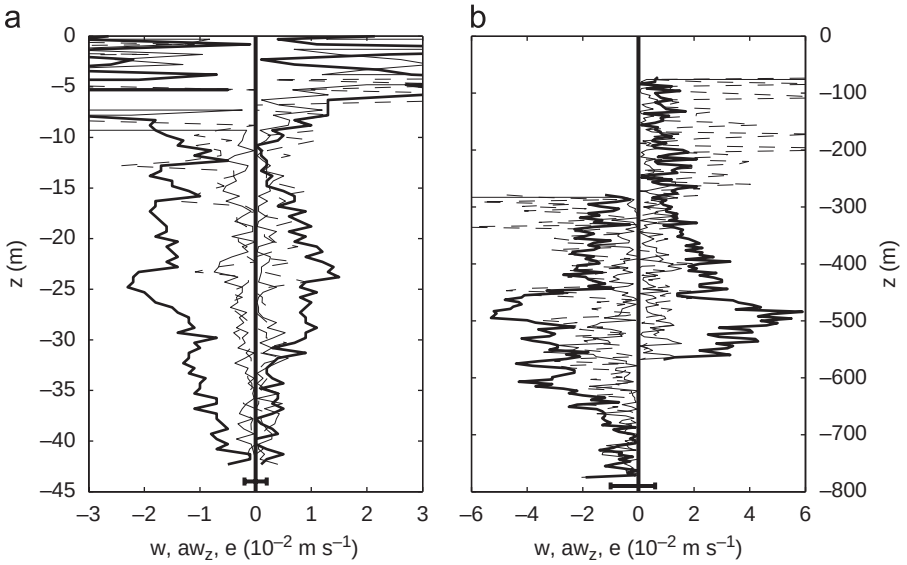

Fig. 1. Test of (A4) using raw data by comparing the second term on the right-hand side ($a\hat{w}_z$; thin dashed lines) with the observed $\hat{w}$- (heavy solid) and $\hat{e}$-estimates (thin solid). Only absolute values are shown (which are made negative in half the occasions for graphic purposes). (a) Two examples from uplooking ADCP, summer-INP, day 194.715 (negative values; large high-frequency wave) and day 194.8135 (positive values; small high-frequency wave). (b) PROCS at H∼800 m, day 274.935 (negative values; large high-frequency wave) and PROCS H∼600 m, day 276.067 (positive values; large near-bottom high-frequency wave). Note the different scales compared to a.

Nevertheless, ADCP's principle of measurement requires some attention to understand the scales resolved, but it offers a direct error estimate 'e' for w (Appendix A; Fig. 1).

Of primary interest here are the particulars in w-observations near the buoyancy frequency N and their correlation with large-scale convection or shear. Traditionally, the internal gravity wave band is defined between frequencies $f<\sigma<N$, where $f=2\Omega\sin\varphi$ represents the vertical component of the Coriolis force, of the Earth rotational vector $\mathbf{\Omega}$ at latitude φ. Outside this frequency range waves are in principle evanescent motions, exponentially decaying in amplitude, except in weak stratification where $N=O(f)$ and the inertio-gravity wave band extends substantially beyond the above limits due to the effects of the horizontal component $f_h=2\Omega\cos\varphi$ (LeBlond and Mysak, 1978).

Near f, motions are predominantly horizontal and near-circular when $N>f$, so that shear in the vertical is "constant" or slowly varying with time. In general, ocean shear is dominated at f, except near an internal tide source like the upper part of continental slopes and in tidal turbulent bottom boundary layers (van Haren et al., 1999).

Near N, motions include at least substantial w, but it can be shown that horizontal circular motions exist exactly at N for any N due to f_h (Gerkema et al., 2008). Obviously, for large $N\geqslant O(10f)$ the amplitude of these horizontal motions becomes very small compared to w, and their circular motion will be hard to detect. Nevertheless, it is interesting to investigate the possible effects of near-circular N-motions on shear, which also have a permanent character in theory, just like f-motions.

Convective overturning is expected over a wide range in time, varying from sub-inertial scales of atmospheric disturbances to tidal scales in a bottom boundary layer. Thus we hypothesize a possible relationship between $w(N)$ and sub-inertial, inertial and tidal scales.

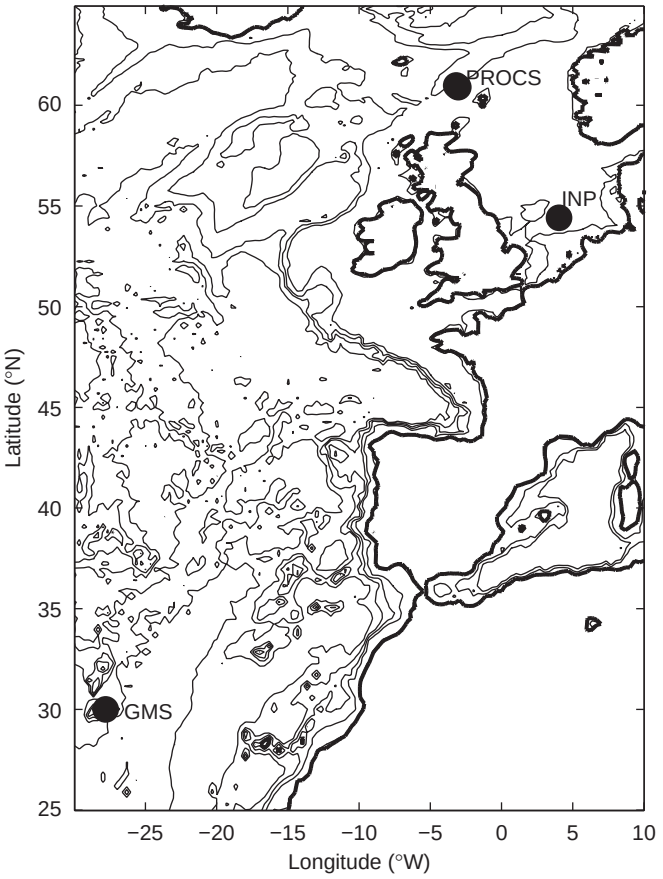

Fig. 2. Mooring locations (●) in North Sea (INP), Faeroe–Shetland Channel (PROCS) and North-Atlantic Ocean bordering the Canary Basin (GMS).

2. Data

Vertical motions are investigated using moored four-beam ADCP-data from a site in the central North Sea in summer 1994 (project INP), from two sites in the Faeroe–Shetland Channel in fall 1999 (PROCS) and from a site near Great Meteor Seamount (GMS), Canary Basin, North-Atlantic Ocean mainly in 2005. Fig. 2 shows mooring locations and Table 1 lists the time intervals of operation. At the INP-site, additional temperature data are obtained using Aanderaa thermistor strings and atmospheric

Table 1
RDI-broadband uplooking-ADCP mooring details.

	INP summer	PROCS4	PROCS7	GMS
Data start	13/07/1994	24/09/1999	24/09/1999	19/10/2004
Data end	21/07/1994	10/10/1999	10/10/1999	15/12/2005
Latitude	54°25′N	60°54′N	60°59′N	30°00′N
Longitude	004°02′E	−003°02′W	−003°11′W	−027°48′W
Water depth (m)	45	600	802	4550
Vertical slant angle (θ)	20°	20°	20°	20°
Transmit frequency	600 kHz	75 kHz	75 kHz	75 kHz
Transmission length	1.9 m	7.7 m	3.8 m	28 m
Instrument depth	0.3 m a above b bottom	17 m ab	17 m ab	3205 m ab
First bin	41.9 m	568 m	774 m	1307 m
# bins × bin size	90 × 0.5 m	125 × 4 m	125 × 4 m	50 × 10 m
Ensemble period	150 s	300 s	300 s	900 s
Std u, v	0.006 m s^{-1}/ens	0.019 m s^{-1}/ens	0.031 m s^{-1}/ens	0.014 m s^{-1}/ens
Std w, e	0.002 m s^{-1}/ens	0.006 m s^{-1}/ens	0.010 m s^{-1}/ens	0.005 m s^{-1}/ens

INP is in the central North Sea, PROCS in the Faeroe–Shetland Channel during fall and GMS represents yearlong data above (the foot of) Great Meteor Seamount in the North-Atlantic Ocean.

conditions are monitored using a fully equipped meteorological buoy, including radiation sensors. These instruments were moored less than 300 m from the ADCP, except for mid-depth temperature sensors that were on a line directly above it.

All ADCPs' motion sensors worked adequately, not being biased by rapid motions like due to surface waves. At INP, the bottom frame moved a little bit due to drag on the thermistor string line: mean ADCP-heading was $10.7 \pm 0.4^\circ$ TN, mean tilt $1.47 \pm 0.13^\circ$. These small variations did not affect w-data. Tilt-data of the other moorings will be presented below, which demonstrate no aliasing of horizontal currents in w-data, not even at low aspect ratio tidal frequencies (see also Appendix A).

3. Observations

Unless otherwise stated, the ADCP-observations presented below are raw, unfiltered data. Henceforth, all tildes of observables in (A1) will be dropped.

3.1. North Sea

In the strongly stratified (Figs. 3 and 4) and likewise sheared (Fig. 4d) summertime central North Sea we investigate the possibility that convective motions in the mixed layer drive the vertical motions in the pycnocline by comparing it to shear that may destroy high-frequency internal waves. Dominant horizontal currents have tidal periodicity in the bottom half of the water column and a mixture of tidal and inertial periodicity in the upper strongly stratified half (van Haren et al., 1999). Tidal motions are weak but visible in w (Fig. 4b). However, they are varyingly related to horizontal currents and hence not associated with instrumental errors (Appendix A). Such tidal variability is not observed in e (Fig. 4c) and always $|w| > |e|$. All tidal motions including those in w are not representing free internal waves but are due to frontal advection, as has also been established differently in previous analyses (van Haren and Maas, 1987; Howarth, 1998). The tidal variation of isotherm displacements is also observed in the frictional bottom boundary, which is thus not always homogeneous (Fig. 3).

The summer period is also characterized by diel plankton migrations, which are most manifest in the ADCP's echo data (Fig. 4e). These diurnal motions are not clearly visible in w, presumably because the vertical range $O(10\,\mathrm{m})$ is so short and migration speeds are rather slow. Otherwise, they would have been easily distinguishable from high-frequency motions.

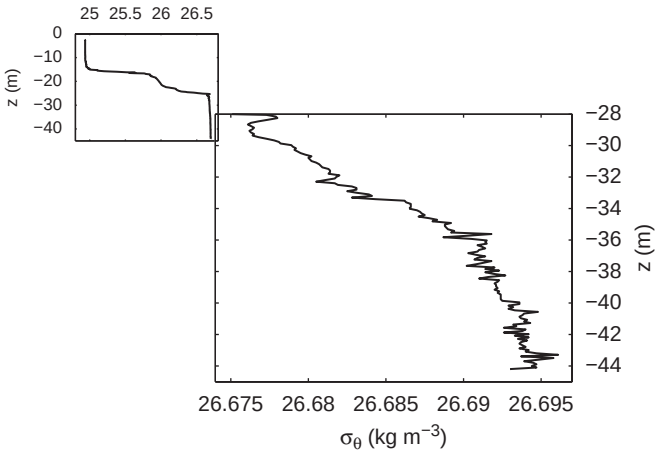

Fig. 3. Example profile of density anomaly obtained on day 197.66 next to the INP-mooring site. The associated buoyancy periods are about 1400 and 2600 s for the ranges [−28, −36] and [−36, −44] m, respectively, whilst 390 s around −20 m.

In terms of vertical density stratification, the frictional near-bottom layer 'persistently' shows a minimum stratification for which the buoyancy frequency $N \approx 5 \times 10^{-4}\,\mathrm{s}^{-1} \approx 4f$ (van Haren, 2004). In this layer, larger stratification resulting in larger N and thus smaller buoyancy periods T_N of less than an hour are observed during particular phases of the tidal current (e.g., Fig. 3). Over the entire water column, vertical density profiles are characterized by two strongly stratified layers at about −15 and −25 m ($T_N \approx 150$–300 s), with weaker stratified layers above and below: the weakly stratified layer in between still shows $T_N \approx 350$–500 s. Near the start of the ADCP-record, on day 194, a flux of nutrients evidencing diapycnal mixing was observed above the upper stratification followed by an increase in near-surface plankton (van Haren et al., 1999). At day 194 w shows very thin lines, representing small-scale internal waves that hitherto went unnoticed (Fig. 4b). These w have amplitudes that are an order of magnitude larger than tidal w. They are significantly distinguished from instrumental error, as found in e (Fig. 1).

Such vertical thin lines are found around mid-depth, e.g. at days 194.8, 198.1, both during nighttime convection (Fig. 4c), and near the bottom, e.g. clearly at days 200.0 and 201.1. The start of the time interval of largest high-frequency motions in the record (day 194.70; Fig. 5), having a period of 1900 ± 100 s, evidences advection before free linear wave propagation prevails from day 194.75 onwards. The latter shorter scale motions have periods of

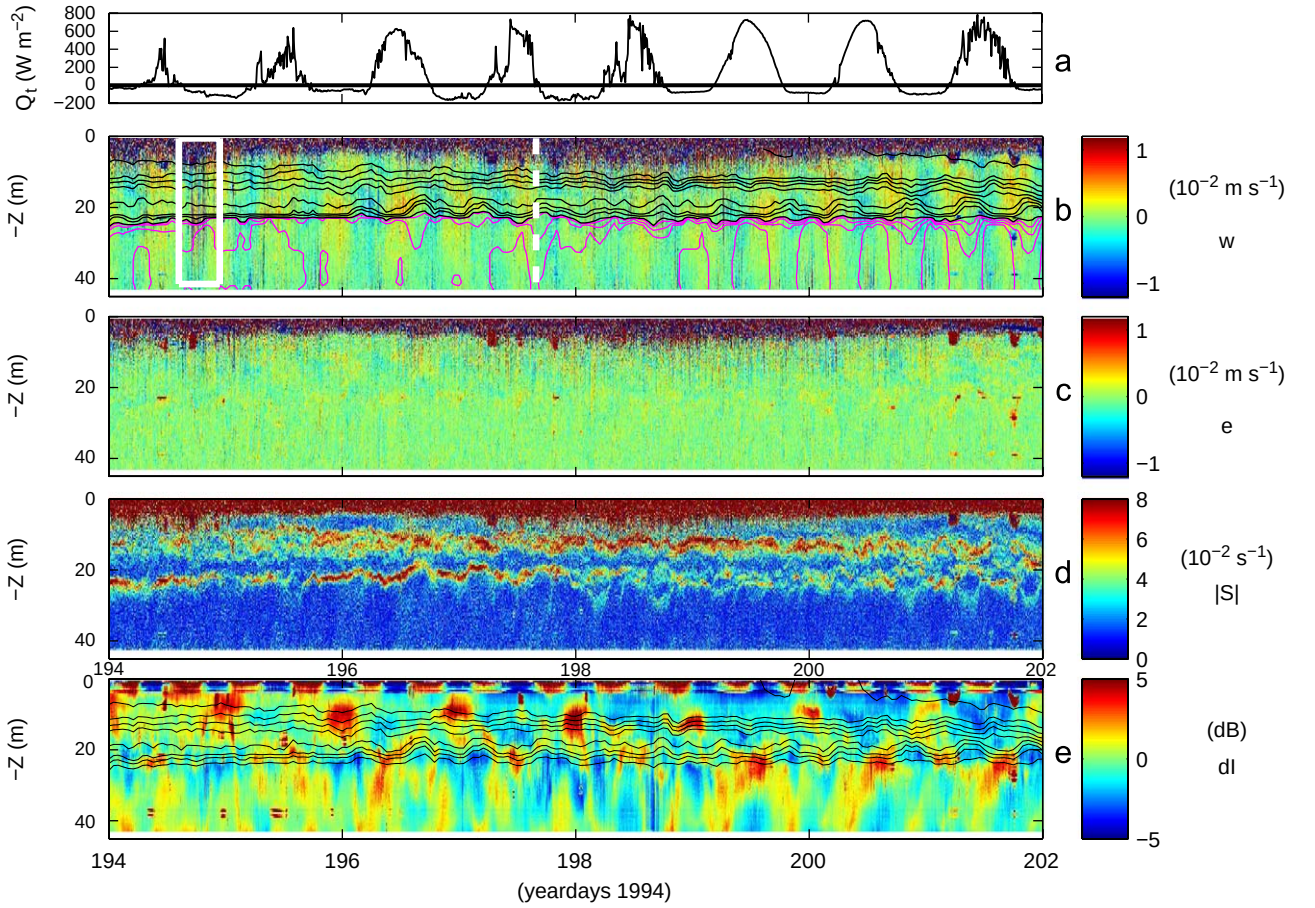

Fig. 4. Overview of summertime INP time series. (a) Total surface heat flux computed from local meteorological data using (B2). (b) Vertical current data with hourly smoothed temperature contours every 1 °C between 10–18 °C (black) and every 0.2 °C between 9.1 and 9.9 °C (purple). The white rectangle indicates the period of Fig. 5, the white line that of Fig. 3. (c) Error velocity data and black contours as in b. (d) Vertical current shear magnitude data (using $\Delta z = 0.5$ m) and black contours as in b. (e) Relative echo amplitude corrected for water attenuation and black contours as in b. In b–d. the brown band and in *e*. the tidal variation between 0 and about −7 m represents bad (surface reflection side-band) data. (For interpretation of the references to colour in this figure legend, the reader is referred to the web version of this article.)

1500 s, with 4 waves in a group, decreasing to 430 s, with 7 waves in a group. These periodicities correspond with the buoyancy period T_N inferred from CTD-profiles (Fig. 3) around −20 m ($T_N = 400$–450 s), and with T_N below and above the layers of strong stratification, the frictional layers, during a phase when tidal turbulence is weak so that frontal advection leads to [re]stratification.

The associated waves, however, appear as mode-1 waves around the layer of strongest stratification, −22.5 m (Fig. 5). The very stripy appearance of w (Fig. 5c) smoothly, ∼linearly decreases its amplitude away from the mid-depth pycnocline, and occasionally away from the surface (from day 194.81 onward). Although no clear change in mode-1 structure is observed in w at the above transition on day 194.75, after the first two 'waves', the sudden shortening in periodicity is accompanied by a just-resolved change to apparent mode-2 in temperature data of the weakly stratified layer below the lower pycnocline ∼−27 m (Fig. 5b). When forming closed contours, such mode-2 motions can transport material.

No clear preference for depression or elevation, typical for solitary waves, is observed for the suddenly appearing group of waves, but this may have to do with the mid-depth occurrence of the motions. The shear magnitude associated with this pycnocline maintains a fairly large minimum value of about $|\mathbf{S}| = 5 \times 10^{-2}\,\mathrm{s}^{-1}$, which is to within 20% equal to the local, thin-layer, buoyancy frequency, but it varies by 50% during the passage of the high-frequency motions. During this passage, the local N also varies by about the same rate, so that between days 194.7 and 194.85 the mean straining is precisely doubled (the temperature difference halved), with a minimum local buoyancy frequency only 70% of the value before the passage. The effects on the upper pycnocline even seem more dramatic: the shear drops by just over a factor of 2 on day 194.7.

This date corresponds with the moment of neutral net radiation, about an hour after total net surface heat flux changes sign (Fig. 5a). The time of highest-frequency motions (day 194.81) corresponds with the time of onset of negative net radiation and further decreasing total heat flux. These moments in time are also reflected in the sudden lengthening of the near-surface buoyancy period from 400–900 to 2000 s (Fig. 5e, blue lines). Despite the fact that observed w is of the same order of magnitude as expected from convection estimates (Appendix B; (B1) or (B2)) and given the above timing, penetrative convection may not be the only direct cause of the high-frequency waves as the maximum w-values are observed at the lower pycnocline, which is not directly affected by diurnal variations in near-surface convection. However, it may be indirectly affected via pressure fluctuations that were not measured.

As for the possibility of lower-pycnocline high-frequency wave generation via turbulence from below: at the top of the weakly stratified near-bottom layer shear is larger than stratification between days 194.7 and 194.76 (Fig. 5e). This corresponds with

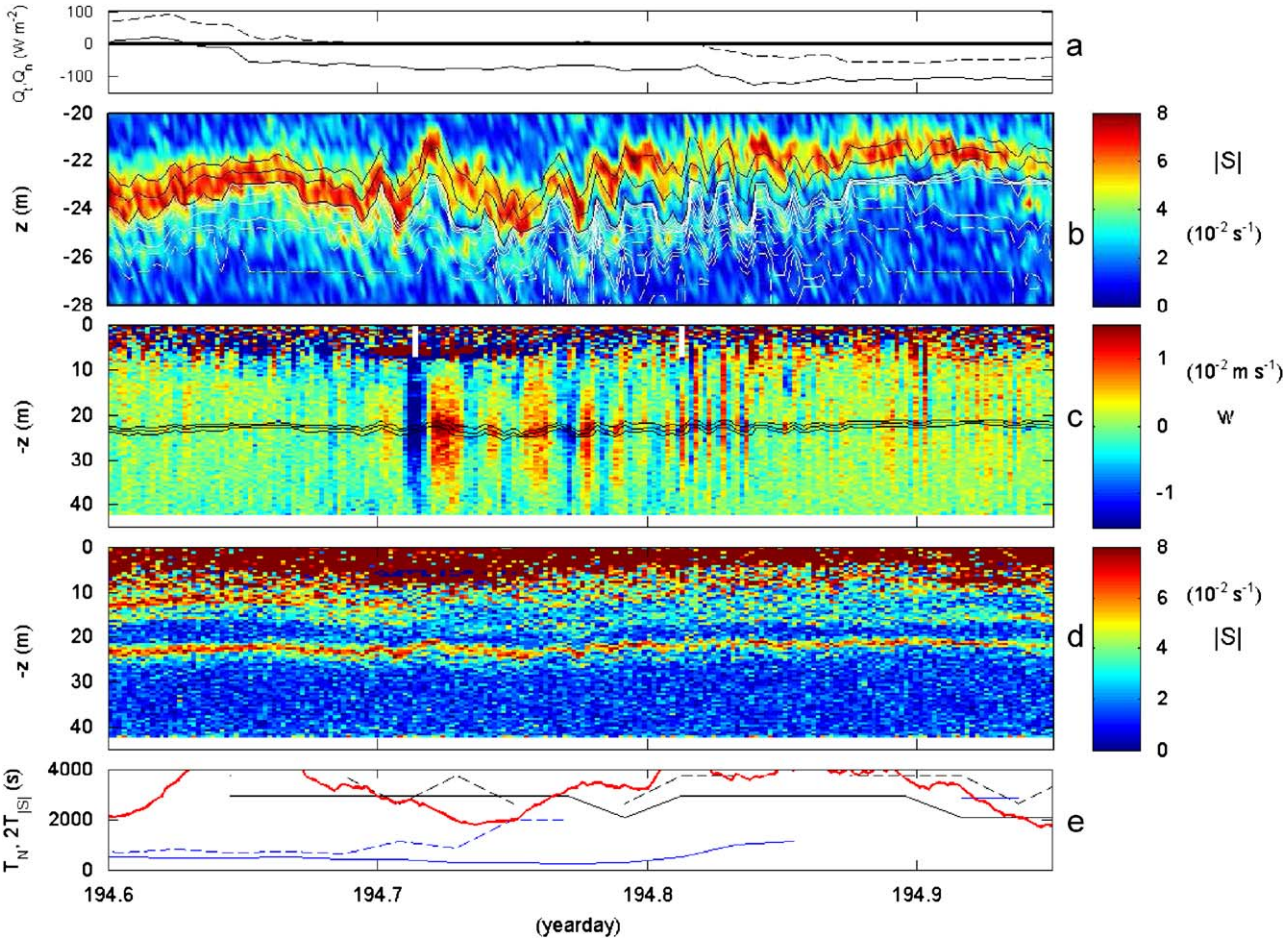

Fig. 5. Detail of 0.35 day of summertime INP time series. (a) Total surface heat flux Q_t (solid graph) and net radiation Q_n (dashed). (b) Lower thermocline detail of graphically smoothed vertical current shear magnitude with unsmoothed temperature contours every 1 °C between 10 and 12 °C (black). In white, contours every 0.1 °C between 9.2 and 9.9 °C, in white-dashed every 0.02 °C between 9.45 and 9.57 °C. (c) Total depth vertical velocity and black contours as in b. Periods of Fig. 1.a are indicated. (d) Total depth unsmoothed vertical current shear magnitude. (e) Bottom "boundary layer" buoyancy period computed using half hourly temperature data between −29 and −39 m (solid black) and between −27 and −43 m (dashed black) in comparison with (twice) the shear period computed using half-hourly smoothed ADCP-data between −30 and −40 m (red). Similarly, in blue, "surface boundary layer" buoyancy period between −3 and −5 m (dashed) and between −3 and −7 m (solid). When no buoyancy period is given the temperature data were identical to within instrumental resolution at the two computational levels. (For interpretation of the references to colour in this figure legend, the reader is referred to the web version of this article.)

the time interval of large non-linear advective motions, prior to arrival of free high-frequency wave motions. It is noted that the waves are likely generated elsewhere, but this is unfortunately unverifiable with the present data-set.

The short time interval in Fig. 5 shows enhanced w-spectral band around N (Fig. 6). The comparison with the e-spectrum shows that the large w is significant, even on the scale of the small local buoyancy period of about 400 s at the interface. In the bottom boundary layer at −40 m also significant N-motions are observed, with a tendency of peak shift to $\sigma > N$ (blue spectrum). This super-buoyancy shift is also found in laboratory models of turbulent bottom boundary layers generating internal waves (Taylor and Sarkar, 2007).

For the entire record, correspondence between high-frequency $|w|$ ($\sigma > 15$ cpd, cycles per day) and low-frequency $|\mathbf{S}|$ ($\sigma < 15$ cpd) is ambiguous (Fig. 7). Higher up in the water column $|w|$ corresponds only moderately with $|\mathbf{S}|$, both are at elevated values with respect to the near-bottom values. There is some face-value correspondence between low-frequency $|\mathbf{S}|$ and the modulation of high-frequency $|w|$ in the upper pycnocline, where inertial shear dominates (Fig. 7, upper panel), and in the bottom boundary layer, where tidal shear dominates (Fig. 7, lower panel). Especially in the latter, a clear tidal modulation is found for high-frequency $|w|$. Despite the largest high-frequency w, there is no correspondence between local $|\mathbf{S}|$ and $|w|$ across the lower pycnocline where the strongest stratification is found. This implies that the high-frequency internal waves are not generated via local shear, but more remotely as suggested above.

3.2. Faeroe–Shetland channel

In the FSC, main stratification is around 400–500 m, centered below mid-depth at both sites (Fig. 8). As the influence of near-surface convection is not expected to be of large influence in directly generating w at this main pycnocline, we investigate general particulars of w in an area of shoaling deep topography. The main stratification occasionally reaches the bottom at 600 m while moving upslope as a vigorous bore (Hosegood et al., 2004). Typical stratification profile at $H \sim 800$ m results in $T_N \approx 1200$–1800 s between 320–550 m and $T_N \approx 3500$–7000 s above and below that layer (Fig. 8).

In the FSC, horizontal current amplitudes amount up to 0.8 m s^{-1}, with large variations in the vertical (Fig. 9). The relatively large currents cause ADCP-tilt up to 10°, with one exception on day 274.6 ($H = 600$ m) when a vigorous near-bottom

bore passed (Fig. 9a). In general, tilt corresponds very well with observed near-bottom horizontal current amplitude. It corresponds only weakly with |**S**| ($\sigma < 15$ cpd) and poorly with $|w|$ ($\sigma > 15$ cpd). For example, some of the strongest high-frequency $|w|$ and low-frequency |**S**| occur during mid-night on days when horizontal currents are also particularly small. These periods will be discussed in detail below.

Despite both detailed examples in Figs. 10 and 11 are periods around mid-night, atmospheric convection is not expected to be important this deep in the FSC. Although a direct correlation between high-frequency $|w|$ and low-frequency |**S**| is not significant, face-value correspondence is reasonable between some of their peaks. These include nighttime peaks and, especially at $H = 600$ m, a tidal-inertial variation in peak heights of $|w|$ that correspond about half the time with peaks in |**S**|. At $H = 800$ m high-frequency $|w|$ seem associated with non-tidal sub-inertial variations, or most likely indirectly with atmospheric disturbances (Hosegood et al., 2004).

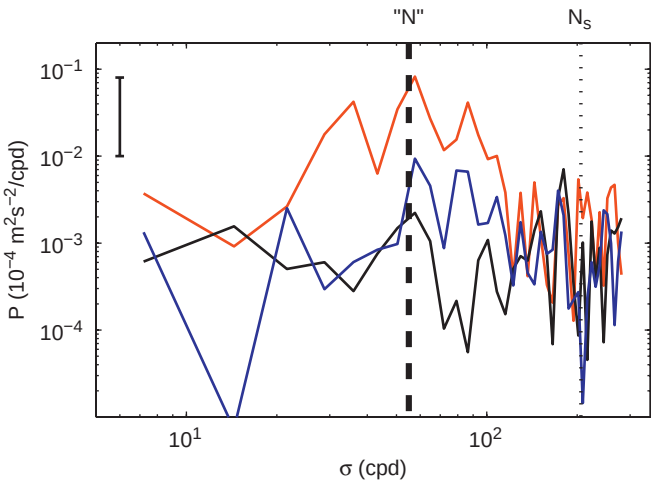

Fig. 6. Detail between days 194.70 and 194.85 of nearly raw w-spectra from summertime INP-data at −22.5 m (red; lower thermocline) and −40 m (blue), with reference e-spectrum corresponding to the latter (black). The heavy dashed line indicates the buoyancy frequency corresponding to a period of 1660 s associated with the bottom boundary layer, while the dotted line indicates a period of 420 s corresponding to strong stratification N_s. (For interpretation of the references to colour in this figure legend, the reader is referred to the web version of this article.)

When considered in detail, similar to INP, vertically striped, generally mode-1, weakly attenuated w-motions are observed in the FSC, albeit occurring in irregular groups across a substantial part of the water column (Figs. 10 and 11). Water depth is an order of magnitude larger than in the central North Sea. Vertical currents associated with high-frequency motions are larger (by a factor of 3–4) than in INP, commensurate with the equally weaker stratification that supports them. Like in the North Sea, maximum $|w|$ are found near the layer of largest shear and stratification, in the FSC around 500 m. The shear is found in thin layers. When shear extends above the noise, its layers coincide with thin layers of enhanced values of ADCP's relative echo intensity dI that is corrected for water attenuation. Commonly, dI is assumed to be a measure of the suspended material or plankton and fish, but it may also reflect 'stratified turbulence', minute motions of temperature-jump surfaces. It is a reasonable substitute for measuring stratification variations where we lack detailed temperature observations as in the present FSC-data. Vertical plankton migration motions are easily distinguishable from the dI-records as they have a predominant diurnal cycle: upward at the end of each day, between day .70 and day .75, downward between day .25 and day .30, especially visible in Fig. 11. By comparing depth-time w-panels (Figs. 10c, 11c) with dI-panels (Fig. 10d, 11d) it is clear that high-frequency w are distinguished from diel plankton migrations.

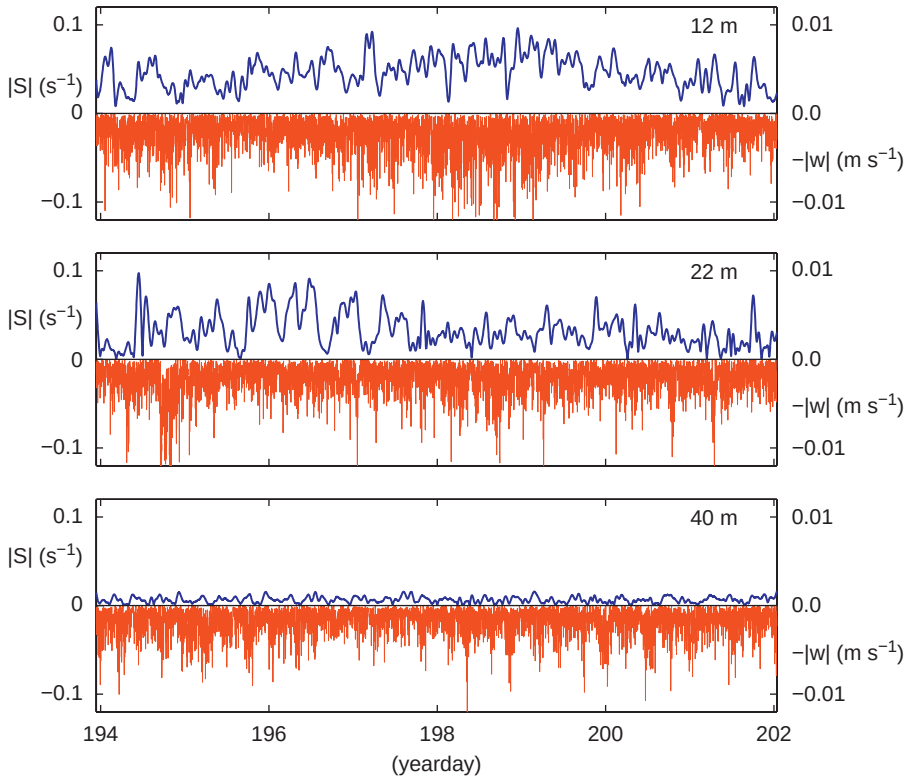

Fig. 7. Time series of band-pass filtered shear ($\sigma < 15$ cpd; blue graph) and vertical current magnitude ($\sigma > 15$ cpd; in red; made negative for display purposes) for 3 depths during INP. (For interpretation of the references to colour in this figure legend, the reader is referred to the web version of this article.)

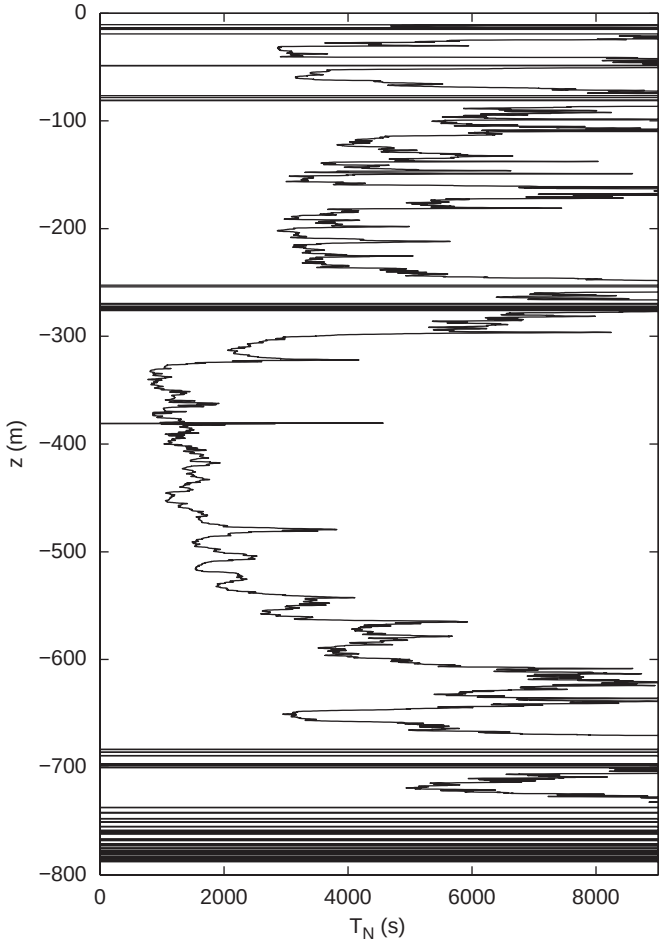

Fig. 8. Example profile of buoyancy period computed over $\Delta z = 10$ m during PROCS.

In H∼800 m (Fig. 10) the initially large wave is, in terms of a passing 'solitary' wave, a wave of depression around −600 and −700 m. According to the w-observations, which do show a mode-2 motion for the first wave, the 'solitary wave' seems to be blocked in the vertical by a shallower pycnocline (−500 m), which supports another train of waves. The latter waves have a much shorter period (2100 decreasing to 1200 s, vs. 4800 s for the first period at −600 m). The minimum value is very close to the minimum $T_N = 1225 \pm 50$ s inferred from the sample density profile (Fig. 8). The group between days 274.81 and 275.06 in Fig. 10 contains 12 waves, of which 8 have the shortest period after the passage of the large wave. The large wave period is associated with maximum $T_N = 5400 \pm 1500$ s, found well outside the pycnocline. At the depth of the pycnocline, where **|S|** (Fig. 10a) and dI (Fig. 10d) occur in thin layers, the short waves apparently have the same horizontal scale as the ADCP's beam spread (100–200 m), because weakly some rare stripes are observed in e as well (Fig. 10b), although over a much shorter range of some 200 m than w-stripes that reach over at least twice that range (Fig. 10c).

Such stripes in e are absent in H∼600 m, where w-stripes can fill nearly the entire water column (Fig. 11). At this site, the main pycnocline approaches the bottom to within a few 10's of meter, possibly governing large sediment resuspension when a favorable 'solitary' wave-(soli)bore passage coincides with the main pycnocline depression. As before, both **|S|** (Fig. 11a) and dI (Fig. 11d) occur in thin layers of vertical extent O(10 m) commensurate CTD-observed N (Fig. 8). In the example of Fig. 11 shown, the associated dI are fairly weak, but comparing short-scale wave variations between days 275.9 and 276.1 in the layers at −100 and −550 m it is observed that they are in phase or just out of phase, so that w-motions are mode-1 or mode-2 across the water column. The number of waves in the group in this time interval is 8, of which 4 have short-periodicity. The first passage resembles a wave of elevation, as expected this close to the bottom. A transition from a depression to elevation wave as

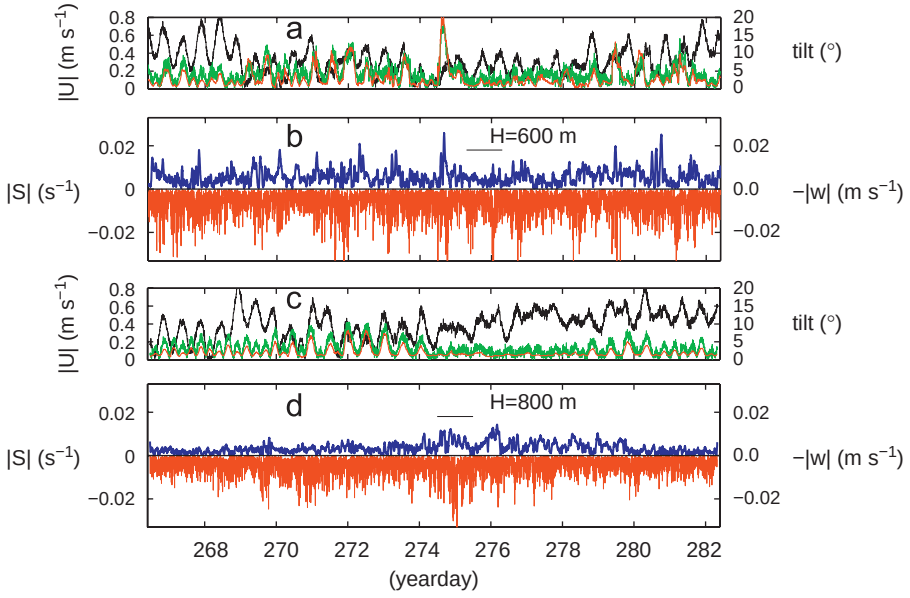

Fig. 9. Total time series of some FSC-data. (a) Current speed at 280 m (black) and 5 m above the ADCP (green) with ADCP's tilt (red; axis to the right) for location $H = 600$ m. (b) As Fig. 7, for data at 540 m ($H = 600$ m). Black bar indicates period of Fig. 11. (c) As a., but for H = 800 m. (d) As b., but for 540 m ($H = 800$ m), with black bar indicating period of Fig. 10. (For interpretation of the references to colour in this figure legend, the reader is referred to the web version of this article.)

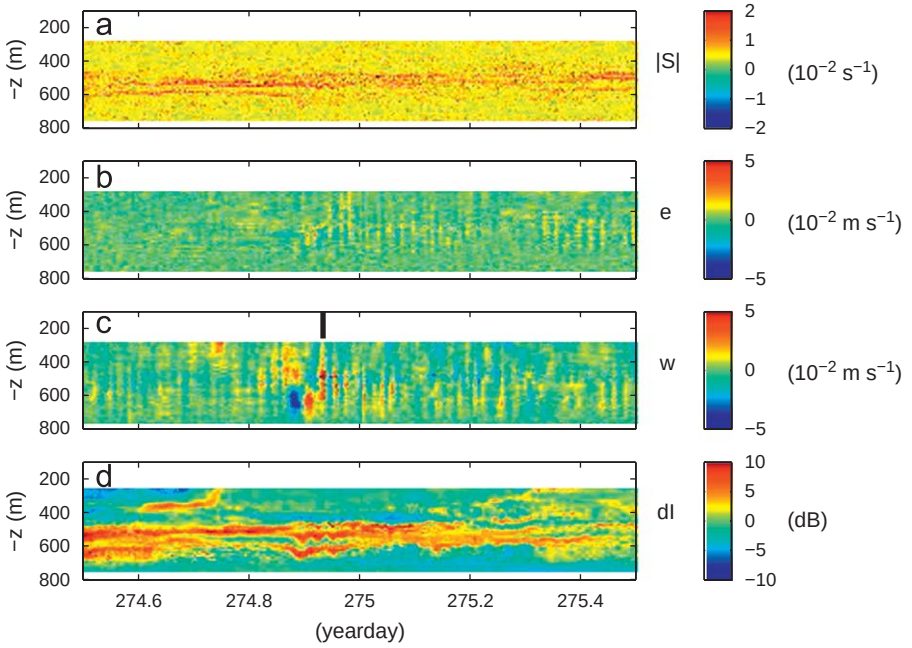

Fig. 10. Similar to Fig. 5 but for 1 day of PROCS-data at H~800 m. (a) Shear amplitude (negative values for colour coding purposes only). (b) Error velocity. (c) Vertical current. Period of Fig. 1.b is indicated. (d) Relative echo amplitude.

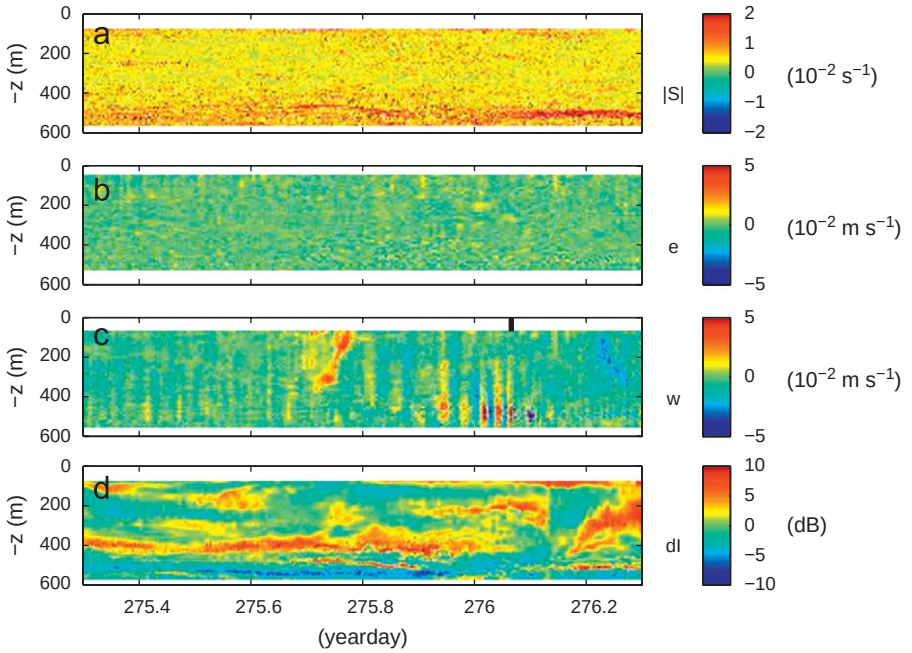

Fig. 11. As Fig. 10, but for 1 day of PROCS-data at H~600 m, different period. Period of Fig. 1b is indicated. Plankton migration is visible between −400 and −100 m around day 275.75 (upward) and 276.25 (downward).

observed near the surface by Orr and Mignerey (2003) is not found in the present deep observations, confirming the notion that separate moorings only 10 km apart horizontally (at $H = 600$ and 800 m) do not completely picture the non-linear wave variability, which has smaller scales.

3.3. Near Great Meteor Seamount

Similar vertically striped w and weak e are also observed in the open ocean, high above the foot of Great Meteor Seamount (Fig. 12). Despite the 3000-m-long mooring, tilt due to drag is small $<1.5^{\circ}$. Compared to FSC-data, in the deep ocean noise is relatively large, scatterers are relatively few, current speed and shear are weaker by a factor of 2 or more, but w near the buoyancy frequency have similar magnitude, again significantly larger than e. One could postulate that high-frequency w is "permanently" observed in the deep. This permanent presence of $w(N)$ implies that the corresponding stratification and shear have a permanent form as well.

Shear is again observed in very thin layers, as thin as the instrumental resolution here, and thinner than observed dI-layers (see detail in Fig. 13). Despite the larger semidiurnal tidal kinetic energy, the shear is entirely dominated at f, which period

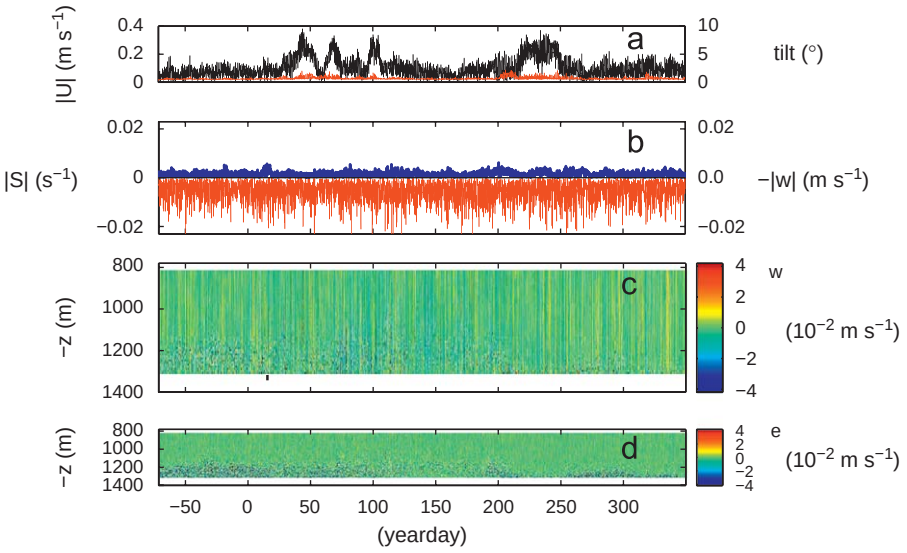

Fig. 12. Total time series of some GMS-data. (a) Current speed at 1000 m (black), with ADCP's tilt (red; axis to the right). (b) As Fig. 9b, for GMS at 1000 m. (c) Raw *w* depth-time series, with black dot indicating period of Fig. 13. (d) Raw *e* depth time-series. (For interpretation of the references to colour in this figure legend, the reader is referred to the web version of this article.)

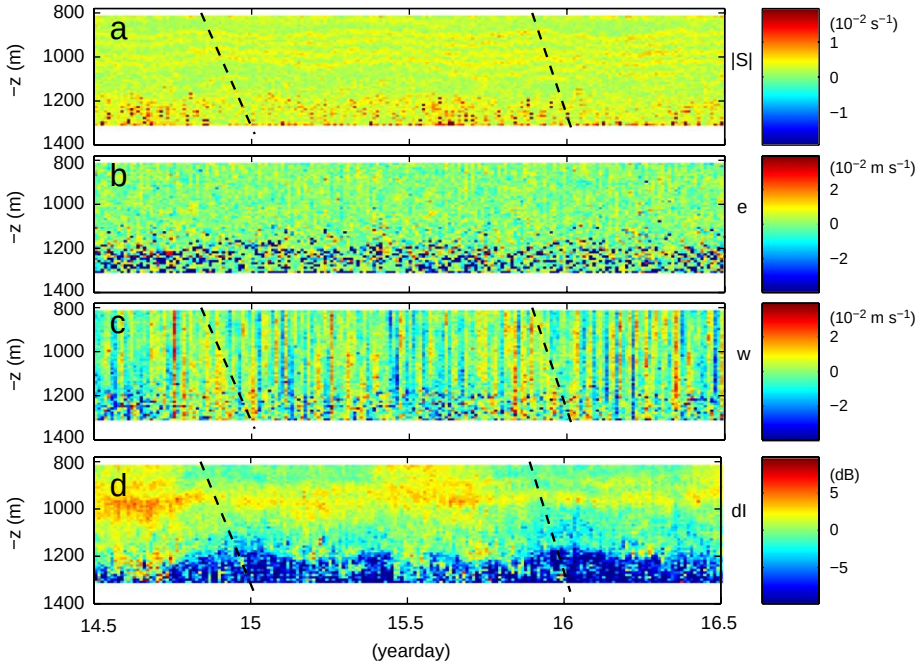

Fig. 13. As Fig. 10, but for 2 days of GMS-data. Period of Fig. 14 is indicated. The lower 100–150 m above the ADCP often show poor data return, presumably due to low scatters amounts.

coincides with the diurnal tidal period here. Diurnal tidal motions have much larger vertical scales and thus smaller shear. Especially the **|S|**-layers often demonstrate small apparent mode-1 waves in terms of vertical excursions, e.g., between days 14.7 and 14.8, between 15.8 and 15.9 and between 16.1 and 16.2, all between 900 and 1100 m. The wave periods vary between 900 and 3000 s, comparable to local buoyancy periods (Fig. 14). Stratification slowly decreases towards the bottom, although many small-scale step-layers are observed throughout the water column. Towards the sea floor $T_N \approx 15000$ s and larger values are found in thin 'homogeneous' layers.

Although within the ADCP's range the small-scale waves seem to be confined between 900 and 1100 m, similar to observations near the surface by Marmorino et al. (1987) although for a much larger layer here, the present *w* show that the apparent mode-1 motions basically range across at least 500 m. Additionally, detailed *w* is layered similarly to layering in **|S|** (e.g., 'profiles' between days 15.8 and 16.3; Fig. 15, but noise is relatively large). This layering compares with INP-data, although a not well-understood phase shift is visible in Fig. 15. A generation periodicity in the small-scale waves is not readily observed, similar to lower-pycnocline INP, but above GMS the

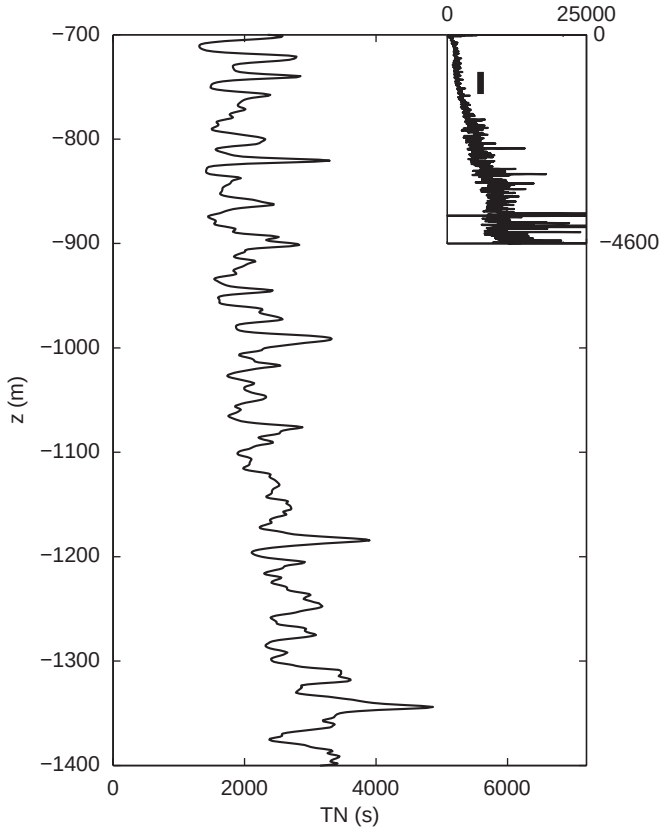

Fig. 14. As Fig. 8 but for GMS during mooring deployment.

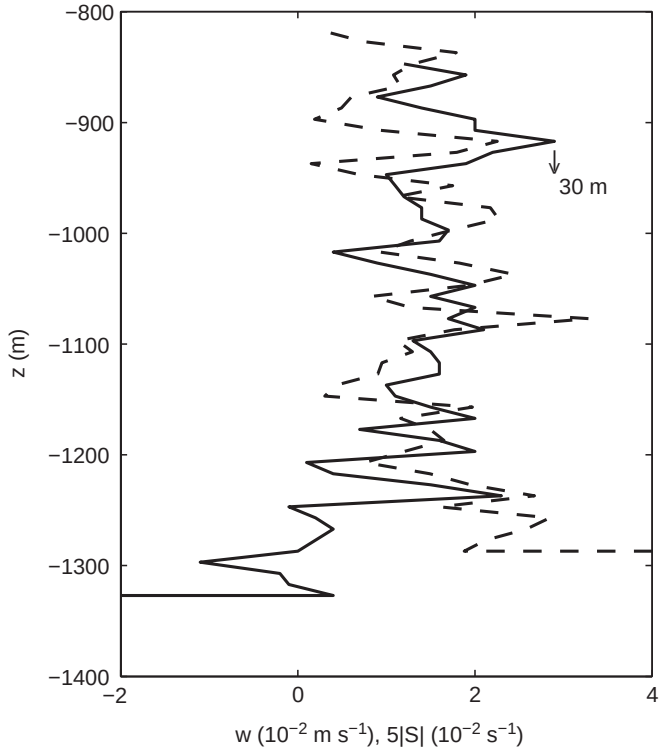

Fig. 15. Instantaneous profiles of GMS-data observed at day 16.17. Note that w (solid) is shifted by 30 m [the length of the arrow] vertically with respect to the shear (dashed) profile. Also note their different scales.

high-frequency w-motions are superposed on vertically forward-slanted [with depth] tidal-w. The yellowish shading implies positive tidal amplitudes in (Fig. 13c). The semidiurnal tidal period is also seen as a modulator in shear- and dI-layers, including the downward phase propagation, which is estimated at 2π-cycle over 1200 m or $\sim$0.025 m s^{-1}. This contrasts with the zero phase changes with depth observed for high-frequency w.

4. Discussion

Vertical current observations using ADCP demonstrate relatively large high-frequency motions close to the buoyancy frequency, both in shallow seas and deep oceans. Although higher frequency motions are barely resolved, it seems that the frequencies of observed w occasionally reach local maximum N while the aspect ratio approaches unity.

As previously observed using temperature data (e.g., Halpern, 1971; Brekhovskikh et al., 1975), high-frequency near-N waves occur infrequently and in small groups, only occasionally with large amplitudes. Overturning as in similar temperature and echo amplitude near-surface observations, e.g., Marmorino et al. (1987), Hebert et al. (1992), Orr and Mignerey (2003), are not observed in the present data, despite some large amplitude O(10–100 m) interface displacements. New in the present observations are the much larger vertical coherent scales of w (and thin interfaces far apart), up to 500 m, the maximum range here.

These vertically coherent, to first-order mode-1, w-motions resemble at first sight very much the deep convection observations by Schott and Leaman (1991). The tests of (A2) and (A4) demonstrate a similar factor of 10 of $|w|$ dominating over $|e|$, also in Schott and Leaman (1991), and the first w-derivative in the vertical employed here. It demonstrates that e is a reasonable estimate for the latter, so that the w-observations describe realistic ocean phenomena that have horizontal length scales larger than the beam spread, being 10 m in the North Sea, and larger than 100 m in the FSC and open ocean. However, the present data do not directly represent free convection, but rather non-linear waves. The association between the motions' periodicity and maximum amplitude with stratification favors an explanation in terms of internal waves.

The vertical extent of w is not unlimited and unusually large although still well less than the water depth. The period of motions is never as small as the local (maximum) buoyancy period computed over $\Delta z < 10$ m, but in the FSC and GMS areas regularly approaches values for T_N computed over 10 m vertical distances. This may be associated with the shear roll-off scale suggested by Gargett et al. (1981). It is unclear whether the large-scale shear-inducing [tidal; inertial] motions generate [mode-2] high-frequency near-N waves. The breaking of such waves seems more following a kinematic rather than a shear-instability (Helfrich, 1992) and the predominant occurrence is more towards neaps when the tidal amplitude is weakest (Marsden et al., 1994; Inall et al., 2001; present North Sea observations).

Also the transfer of energy to high-frequency internal gravity waves by penetrative convection seems largest when the temperature gradient is weak (Stuhl, 1976). Laboratory experiments of the generation of internal waves by vertically moving buoyant fluid demonstrate waves at frequencies 0.25–1.0 N, with particle motions only rarely moving straight-line vertically and more commonly along $\frac{1}{3}$ open ellipses at an aspect ratio between $\frac{1}{3}$ and $\frac{2}{3}$ (McLaren et al., 1973). Recent modeling by Taylor and Sarkar (2007) demonstrates boundary layer turbulence generating pycnocline waves at frequencies just higher than interior-N, with penetrative super-N w as observed here, together with waves

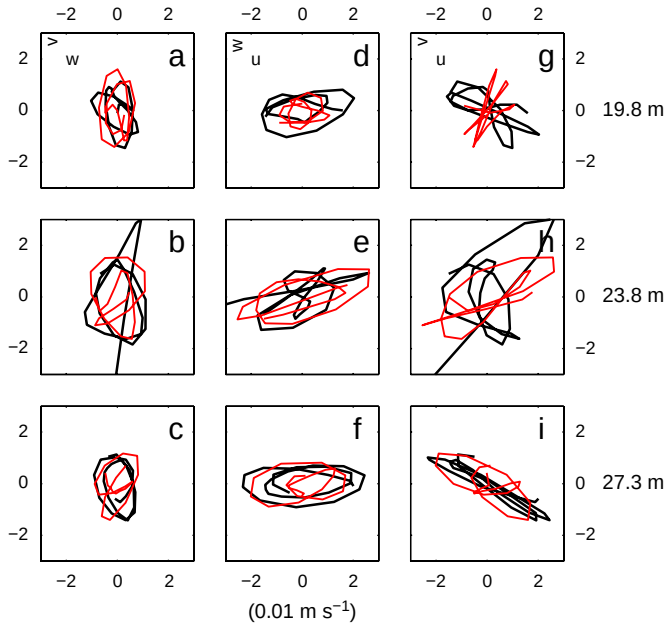

Fig. 16. Current ellipses from band-pass [43, 100]cpd filtered INP-data observed at 3 different depths between days 194.7 and 194.75 (black) and between 194.75 and 194.79 (red). (a–c) w vs. v. (d–f) u vs. w. (g–i) u vs. v. (For interpretation of the references to colour in this figure legend, the reader is referred to the web version of this article.)

propagating into the interior at angles of 35–60°. These angles were previously found in similar experiments for motions at frequencies between 0.5 and 1.0 N (Dohan and Sutherland, 2003). The present observations show a similar ellipticity together with a smaller mean aspect ratio between $\frac{1}{4}$ and $\frac{1}{3}$ (Fig. 16). The large variability with time requires further study and higher resolution detailed observations. In general, much longer time series $O(1)$ year sampled at a rate $O(1–10)$ s are needed to improve statistical and dynamical knowledge of high-frequency non-linear waves and motions.

5. Conclusions

- Series of high, near-N-frequency motions show either mode-1 or mode-2 vertical currents spanning a substantial part, if not all, of the water column. Although the 'waves' have small horizontal extent, they are coherently measured in the vertical using relatively large $O(10–100)$ m horizontally spread instrumentation. This spread amounts $O(0.1)$ times the local water depth.
- The vertical currents decrease more or less linear from the pycnocline of generation, commensurate with theoretical constraints to vanish at surface and bottom because of the boundary conditions, and partially penetrating frictional near-surface or -bottom layers. This may explain the observation of a wave of depression where the main pycnocline is well below mid-depth.
- Thin high-N and $|\mathbf{S}|$ layers show the same layering as w-maxima, both in shelf seas and the ocean. This suggests a direct coupling between inertial, tidal shear and high-frequency internal waves.

Acknowledgments

The assistance of the crew of R/V Pelagia is highly appreciated. Margriet Hiehle made Fig. 2. Theo Hillebrand provided indispensable assistance in mooring preparation. Integrated North Sea Program (INP), Processes above Continental Slopes (PROCS) and Long-term Ocean Climate Observations (LOCO, some of which are the GMS-observations) were funded in part by the Netherlands Organization for the advancement of Scientific Research (NWO).

Appendix A. Observing vertical currents using ADCP

The measurement of high-frequency w using ADCP has several possible shortcomings that need to be addressed for proper error estimates. It is noted that although most of the error estimates given below are valid for any w observed by ADCP, the focus in this paper is on short-scale w near the local buoyancy frequency N. Internal wave near such frequency generally have the largest $|w|$ in the ocean, comparable with vertical motions due to free convection, e.g., in chimneys during deep convection. Near N, horizontal motions are generally weak, $|U| \sim\leqslant O(|w|)$. As a result, contamination of $w(N)$ by horizontal motions is negligible in ADCP-data. This may be different at the low-frequency side of the internal wave band, near inertial f and tidal D_2 frequencies, where $|w|/|U| = O(0.1–0.01)$. The observed effect on $w(f, D_2)$ will be considered briefly at the end of next paragraph.

We consider an ADCP with four beams numbered $i = 1, \ldots, 4$, at 90° angles from each other in the horizontal plane and which are slanted at an angle θ with respect to the vertical z (RDI, 1992). Here, $\theta = 20°$, so that the instrument favours the measurement of w over u, v by about a factor of 3.4 and errors due to refraction of the acoustic beam by stratification are negligible. Velocity is only measured in the beam directions. Each of the four "beam velocities" b_i can be decomposed into a vertical component w_i and one of the horizontal components $u_{1,2}$ or $v_{3,4}$. Depending on the mooring configuration, the system can be tilted up to 20° before the compass shuts down and data become unreliable. Such tilts do not affect high-frequency w-measurements, because of the relatively weak horizontal currents at these frequencies and because an ADCP adequately corrects each individual sample using its intrinsic tilt [and heading] sensors when unbiased by fast motions like surface waves. To verify this, we consider tidal motions for which $|w|/|U| \approx 5 \times 10^{-3}$, very low, and for which a tilt bias of only a few 0.1° already would result in 100% error in w.

In Fig. 17 it is observed that tidal-w, due to frontal advection and not representing free internal waves, do have maxima at depths where $|U|$ is maximal as well. However, the $|w|$- and $|U|$-profiles increase differently with height above the bottom, especially in the lower half of the water column, for different phases of the tide with similar amplitudes. As a result, the aspect ratio-profiles can be completely reversed, which cannot be due to an error in tilt of the instrument, which has the same effect over the entire depth range. Surely, if tilt does not affect $w(D_2)$, it certainly does not affect motions at N, which have a much higher aspect ratio. The same is found for the other buoy-mounted ADCP's in this study, see figures with tilt variations with time, which are not related with high-frequency w-time series.

Furthermore, an adequate direct error estimate to $w(N)$ is provided by a four-beam ADCP, which includes errors due to tilt bias and inhomogeneous currents over the beam spread. For an instrument fixed in space the equations for the two "vertical velocity" component estimates read, averaged over the beam spread per acoustic ping and depth level

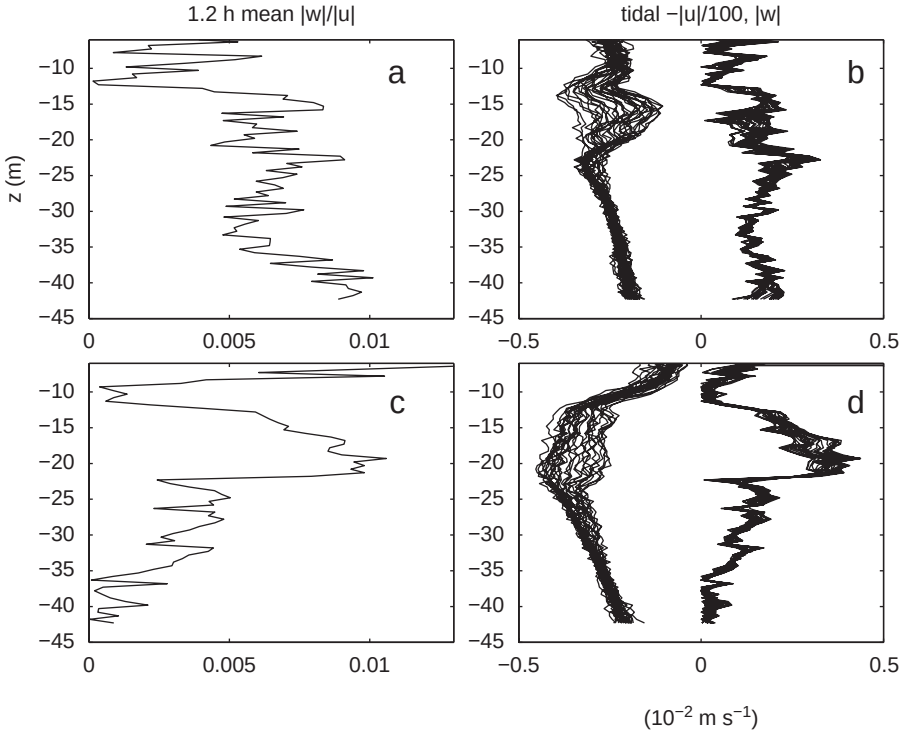

Fig. 17. Verifying w-contamination due to tilt for small-aspect ratio tidal frequency motions using INP-data. (a) Mean aspect ratio $|w|/|U|$ for period 196.73–196.78 (maximum West-current). (b) All profiles for period in a., left: $-|U|/100$, right: $|w|$. (c) As a., but for period 196.45–196.50 (maximum East-current). (d) As. b., but for period in c.

(van Haren et al., 1994),

$$\begin{aligned}\tilde{w} = & -\sum_{i=1}^{4} b_i/4\cos\theta = \sum_{i=1}^{4} w_i/4 + [(u_1-u_2)\\ & +(v_3-v_4)](\tan\theta)/4 \equiv w+\delta w\\ \tilde{e} = & -[b_3+b_4-(b_1+b_2)]/4\cos\theta = [w_3+w_4-(w_1+w_2)]/4\\ & +[(v_3-v_4)-(u_1-u_2)](\tan\theta)/4 \equiv \delta e, \end{aligned} \quad \text{(A1)}$$

in which instrumental noise is not considered and the tilde indicates the measured quantities. The second "error velocity" equation is redundant, as four separated beams are used to estimate only three Cartesian velocity components, but it is useful as it provides an independent indication of the instrumental errors and current homogeneity over the beam spread (RDI, 1992; van Haren et al., 1994). If properly scaled as in (A1), the error velocity $\tilde{e}$ gives a direct estimate of $\tilde{w}$.

In order to understand what the consequences of variations in $\delta(u, v)$ across the beam spread are for $(\tilde{w}, \tilde{e})$, we rewrite,

$$u_1 - u_2 \approx 2\delta x \frac{\partial u}{\partial x},$$

and similarly for the y-direction. If we define half the spreading distance of the beams by $\delta x = \delta y = h\sin\theta = d$, where h measures the distance above the instrument, we find,

$$\begin{aligned}\tilde{w} &\approx w + \left[\frac{\partial u}{\partial x} + \frac{\partial v}{\partial y}\right] d(\tan\theta)/2\\ \tilde{e} &\approx \left[\frac{\partial v}{\partial y} - \frac{\partial u}{\partial x}\right] d(\tan\theta)/2, \end{aligned} \quad \text{(A2)}$$

which shows that an ADCP "measures" several straining components, i.e. divergence in $\tilde{w}$ and shear straining in $\tilde{e}$ that are not necessarily equal in sign.

However it cannot measure the vorticity component,

$$\zeta = \frac{\partial v}{\partial x} - \frac{\partial u}{\partial y}, \quad \text{(A3)}$$

which is a purely tangential quantity.

It is possible however, to verify the principle difference between additional "sampling" in $\tilde{w}$ with respect to that in $\tilde{e}$. If we invoke $\nabla\cdot\mathbf{u} = 0$, the ratio of the terms on the right hand side of the w-equation in (A2) depends on the vertical scale height over which w varies, in combination with θ. If we take as a first guess a distance h for the vertical scale height, we find that the "unwanted" variability in w measures only $O(10^{-1})w$. This can be tested, following van Haren et al. (1994) for heat flux data, when the w-estimate in (A2) is written as,

$$\begin{aligned}\tilde{w} &\approx w - \left(\frac{\partial \tilde{w}}{\partial z}\right) d(\tan\theta)/2 - \left(\frac{\partial^2 w}{\partial z^2}\right)(d(\tan\theta)/2)^2 + \ldots\\ &\equiv w - a\tilde{w}_z - b(w_z)^2 + \ldots, \end{aligned} \quad \text{(A4)}$$

so that the first-order truncation can be justified using measured quantities by comparing the left hand side with the second term on the right hand side. Examples are shown in Fig. 1. In general, the ratio is somewhat larger than expected, and dependent on h as expected from a in (A4), albeit smaller than one and indeed $O(10^{-1})$ at depths where large w-estimates are observed. This gives an idea of the amount of divergence accidentally sampled in the w-estimate at the frequency of the motions of interest. In order of magnitude it is not greatly different from the straining quantities, as the profile of $\tilde{e}$ corresponds largely with that of the term $a\tilde{w}_z$.

Two types of short-scale w-motions, possibly contaminated by divergence, are of particular interest here: those generated as internal waves near the local buoyancy frequency, and those generated following free convective penetration. Note that these velocities are not very small, they vary between 0.01 and

$0.06\,m\,s^{-1}$ (Fig. 1). The examples are taken from high-frequency waves, near N, although not local short-scale N (cf., Section 3). The results compare well with a quick back-of-the-envelope calculation: waves with 1000 s period, phase speed $0.1\,m\,s^{-1}$ have a horizontal wavelength of 100 m, which should indeed be resolved by beams spread apart 20 m, on average.

Appendix B. Vertical motions due to cooling of the sea

As we are concerned with w-observations in, e.g., shallow seas, we consider free convection mainly generated via cooling at the surface. Such turbulence generation results in a particular pattern of vertical convection, eventually under the evolutionary influence of rotation. All the relevant quantities may be expressed in terms of two scaling parameters, the buoyancy flux through the surface B_0 and vertical scale height h_0 (Coates and Ivey, 1997), or B_0 and the systems' frequency of rotation, inertial frequency f (Maxworthy and Narimousa, 1994).

Following a negative surface buoyancy flux, turbulence is generated near the surface and entrains firstly until $t \sim f^{-1}$, to a particular depth. Secondly, rotation influences the turbulence, which results in two-dimensional vortices or plumes reaching down from the transition depth z_c, the near surface fully turbulent region. After interaction with the bottom, the vortex structures fill and tilt and eventually the entire vortex "column" spreads near the bottom and generates baroclinic unstable eddies that shed off the main structure.

When $z_c \approx \gamma(B_0/f^3)^{1/2} < H$, H denoting the water depth and $\gamma = 13$ in Maxworthy and Narimousa (1994) and $\gamma = 35$ in Coates and Ivey (1997), the associated convective speed in the vertical is determined as,

$$w \approx \beta(B_0/f)^{1/2},\ \beta = 1 - 2. \tag{B1}$$

Estimating $B_0 \approx -g\alpha Q_t/\rho c_p$, where g represents the acceleration of gravity, $c_p = 4 \times 10^3\,J\,kg^{-1}\,{}^{\circ}C^{-1}$ the specific heat, ρ the density of water, $\alpha = (1.4(T-6)+3.1) \times 10^{-5}\,{}^{\circ}C^{-1}$ the thermal expansion coefficient, we need only a value of total heat flux of $Q_t \sim -20\,W\,m^{-2}$ for $z_c < H$ in a shallow sea, using the factor as found from the laboratory experiments by Maxworthy and Narimousa (1994). Such Q_t-value is observed nearly every night (Fig. 4a), using a standard parameterization scheme consisting of net solar and long-wave in- and outgoing radiation Q_n, sensible heat flux H_s and latent heat flux LE,

$$Q_t = Q_n - H_s - LE = Q_n - C|W|\rho_a c_p(T_w - T_a) - LC|W|/(R_v T_a) \times (1 - rh)(1200 + (T_a/10 - 1) \times 1100), \tag{B2}$$

where "drag coefficient" $C \approx 1.3 \times 10^{-3}$, $|W|$ denotes wind speed, L evaporation of heat, subscript a indicates air and w indicates water, $R_v = 461\,m^2\,s^{-2}\,K^{-1}$ the gas constant and rh represents fractional relative humidity with values between [0, 1]. As a result, the parameter range leading to w in (B1) is valid for [very] deep-water formation and not for shallow seas, which requires different parameterization.

When $z_c > H$ as in shallow seas, the turbulent layer spreads through the entire water column prior to the development of rotational influence, and hence, the development of distinct two-dimensional vortices. Vertical speeds are then (Coates and Ivey, 1997),

$$w \approx 0.5(B_0 H)^{1/3}, \tag{B3}$$

which amounts $O(10^{-2})\,m\,s^{-1}$ for typical B_0 and $H = O(100)\,m$.

Observationally, in the convective deep areas of the Western Mediterranean Sea, w-observations that were found coherent over several 100 m in the vertical (entire low-frequency ADCP-range) are suggested evidence of deep convection (Schott and Leaman, 1991). Typical values of $|w| = 0.01$–$0.1\,m\,s^{-1}$ are observed, while $|e|/|w| \approx 0.1$.

References

Brekhovskikh, L.M., Konjaev, K.V., Sabinin, K.D., Serikov, A.N., 1975. Short-period internal waves in the sea. Journal of Geophysical Research 80, 856–864.

Coates, M.J., Ivey, G.N., 1997. On convective turbulence and the influence of rotation. Dynamics of Atmosphere and Oceans 25, 217–232.

Dohan, K., Sutherland, B.R., 2003. Internal waves generated from a turbulent mixed region. Physics of Fluids 15, 488–498.

Gargett, A.E., Moum, J.N., 1995. Mixing efficiencies in turbulent tidal fronts: results from direct and indirect measurements of density flux. Journal of Physical Oceanography 25, 2583–2608.

Gargett, A.E., Hendricks, P.J., Sanford, T.B., Osborn, T.R., Williams, A.J., 1981. A composite spectrum of vertical shear in the upper ocean. Journal of Physical Oceanography 11, 1258–1271.

Gerkema, T., Zimmerman, J.T.F., Maas, L.R.M., van Haren, H., 2008. Geophysical and astrophysical fluid dynamics beyond the traditional approximation. Reviews of Geophysics 46, RG2004.

Halpern, D., 1971. Observations on short-period internal waves in Massachusetts Bay. Journal of Marine Research 29, 116–132.

Hebert, D., Moum, J.N., Paulson, C.A., Caldwell, D.R., 1992. Turbulence and internal waves at the equator. Part II: details of a single event. Journal of Physical Oceanography 22, 1346–1356.

Helfrich, K.R., 1992. Internal solitary wave breaking and run-up on a uniform slope. Journal of Fluid Mechanics 243, 133–154.

Hosegood, P., Bonnin, J., van Haren, H., 2004. Solibore-induced sediment resuspension in the Faeroe–Shetland Channel. Geophysical Research Letters 31, L09301.

Howarth, M.J., 1998. The effect of stratification on tidal current profiles. Continental Shelf Research 18, 1235–1254.

Inall, M.E., Shapiro, G.I., Sherwin, T.J., 2001. Mass transport by non-linear internal waves on the Malin Shelf. Continental Shelf Research 21, 1449–1472.

Klymak, J.M., Moum, J.N., 2003. Internal solitary waves of elevation advancing on a shoaling shelf. Geophysical Research Letters 30 (20), 2045.

LeBlond, P.H., Mysak, L.A., 1978. Waves in the Ocean. Elsevier, Amsterdam.

Marmorino, G.O., Rosenblum, L.J., Trump, C.L., 1987. Fine-scale temperature variability: the influence of near-inertial waves. Journal Geophysical Research 92, 13,049–13,062.

Marsden, R.F., Paquet, R., Ingram, R.G., 1994. Currents under land-fast ice in the Canadian Arctic archipelago. Part 1: vertical velocities. Journal of Marine Research 52, 1017–1036.

Maxworthy, T., Narimousa, S., 1994. Unsteady, turbulent convection into a homogeneous, rotating fluid, with oceanographic applications. Journal of Physical Oceanography 24, 865–887.

McLaren, T.I., Pierce, A.D., Fohl, T., Murphy, B.L., 1973. An investigation of internal gravity waves generated by a buoyantly rising fluid in a stratified medium. Journal of Fluid Mechanics 57, 229–240.

Orr, M.H., Mignerey, P.C., 2003. Nonlinear waves in the South China Sea: observation of the conversion of depression internal waves to elevation internal waves. Journal of Geophysical Research 108 (C3), 3064.

RDI, 1992. A Practical Primer. RD Instruments, San Diego.

Schott, F., Leaman, K.D., 1991. Observations with moored acoustic Doppler current profilers in the convection regime in the Golfe du Lion. Journal of Physical Oceanography 21, 558–574.

Stuhl, R.B., 1976. Internal gravity waves generated by penetrative convection. Journal of Atmospheric Sciences 33, 1279–1286.

Taylor, J.R., Sarkar, S., 2007. Internal gravity waves generated by a turbulent bottom Ekman layer. Journal of Fluid Mechanics 590, 331–354.

Thorpe, S.A., 1987. Current and temperature variability on the continental slope. Philosophical Transactions of the Royal Society A 323, 471–517.

van Haren, H., 2004. Current spectra under varying stratification conditions in the central North Sea. Journal of Sea Research 51, 77–91.

van Haren, H., Oakey, N., Garrett, C., 1994. Measurements of internal wave band eddy fluxes above a sloping bottom. Journal of Marine Research 52, 909–946.

van Haren, H., Maas, L., Zimmerman, J.T.F., Ridderinkhof, H., Malschaert, H., 1999. Strong inertial currents and marginal internal wave stability in the central North Sea. Geophysical Research Letters 26, 2993–2996.

van Haren, J.J.M., Maas, L.R.M., 1987. Temperature and current fluctuations due to tidal advection of a front. Netherlands Journal of Sea Research 21, 79–94.